CHARACTERISATION OF CONTACT PRESSURE DISTRIBUTION IN BOLTED JOINTS

M.B. MARSHALL*, R. LEWIS, R.S. DWYER-JOYCE,

Department of Mechanical Engineering, The University of Sheffield, Mappin Street, S1 3JD

*Corresponding author (Tel. (0114) 2227771, Fax. (0114) 2227890)

Abstract

The quantification of contact area and pressure distribution in a bolted joint is essential information, as it determines the integrity of the coupling. Current bolted joint design standards are based on analytical solutions of the pressure distribution, which, due to the inherent assumptions, frequently do not accurately represent the real conditions in a joint.

This study uses a non-intrusive ultrasonic technique to quantify the contact pressure distribution in a bolted connection. The advantage of this experimental technique is that the effect of actual contact conditions can be determined. An ultrasonic wave is focused onto the clamped interface, and the reflected sound signal recorded. In areas where the contact pressure is high, most of the ultrasound is transmitted, and the reflected sound signal is weak. Whereas, when the contact pressure is low the vast majority of the ultrasound is reflected back. A parallel experimental calibration is then used to find the relationship between the reflected sound signal and contact pressure. In this way the pressure distribution in a clamped interface is determined for a series of different bolt torques.

Two different interfaces were investigated; the first consisted of two ground surfaces clamped together, and the second a turned profile pressed against a ground surface. The effect of a washer underneath the bolt head was also considered. The turned profile was found to cause the contact to spread; there was also a certain degree of fragmentation leading to higher peak pressures than in the ground interface case. With a washer positioned under the bolt head for the turned case, the clamping performance of the bolt was improved.

Good agreement was found when comparing the ultrasonic measurements to previous studies, with respect to the spread of the contact pressure distribution. However, in this study the peak contact pressure was found to occur away from the edge of the bolt hole, and to be influenced by the edge of the bolt head.

Keywords: bolted joints, contact pressure

1 Introduction

Bolts are a commonly used mechanical attachment mechanism due to their simplicity and low cost. They are used in many different engineering situations, and can take on a wide variety of forms. When using a bolt to connect two or more components, it is essential that the correct type be used to ensure the integrity of the joint. The integrity of bolted connections has been the focus of many previous research investigations. To date the work has been focused on two key areas; firstly the stiffness of the bolted joint and its response to loading, and secondly the geometry and magnitude of the contact pressure distribution in a clamped interface [1-8]. The interface pressure distribution is required when calculating the clamping performance of the bolt and the joint stiffness. It is also used when assessing the fatigue life of the connection (for example calculation see [1]), along with its ability to conduct thermal energy [2].

Previous work on bolted joints has principally used elastic analytical models or numerical techniques. Fernlund [3] and Greenwood [4] both propose elastic solutions as a design tool for analysing bolted joints. However, these studies both make use of the assumption that the two bolted plates can be considered identical to a single plate of the same combined thickness. Similarly, Gould & Mikic [5] developed a numerical model giving contact pressures in a clamped interface, but in this case with over simplified external load conditions. They neglected to model the bolt in the contact, but rather loaded the joint using a distributed surface load representative of the pressure under the bolt head. The finite element work of Ziada [6], looked to combine a case of two clamped plates along with a more realistic external load condition, this was met with some success. The study showed the importance of the bolt geometry on the interface pressure distribution, and the necessity of including it in the finite element model.

Clearly an experimental technique is required for determining the interface pressure distribution in a bolted joint to verify these numerical models.

Recent experimental research work within this area has made use of pressure sensitive films and pins. However, such methods can change the interface conditions and pressure distribution, as demonstrated by the work of Sawa et al. [7]. The aim of this work is to use a non-intrusive ultrasonic based technique to quantify the interface pressure distribution between two bolted plates. A similar method was used by Ito [8] to analyse the contact at widely spaced discrete points on a bolted interface. However, the technique was limited by poor spatial resolution, extrapolation of the determined pressure distribution, and by an assumption of linearity when relating the ultrasonic measurements to contact pressures. In this study the work is advanced by ultrasonically scanning a bolted interface, and by using a specific parallel experimental calibration procedure to relate these reflections to contact pressure. The interface pressure distributions determined in this study will be a useful tool for assessing the integrity of bolted joints, along with the factors that influence it.

2 Ultrasound and Rough Surface Interfaces

All real engineering surfaces are to some degree rough. As shown by the example surface in Figure 1a, the roughness profile is attributable to asperities distributed all over it. When two surfaces are pressed together contact occurs at these asperities with air gaps in between, this results in an incomplete interface between the bodies. If a normally incident ultrasonic sound wave is directed at such an interface, it is transmitted through the regions of asperity contact and reflected at the air gaps (Figure 1b). This relationship is limited to the case of normally incident ultrasound, with a different result

gained for the case of obliquely incident sound waves. The reflection coefficient, *R*, is defined as the fraction of the ultrasonic wave incident at the interface that is reflected from it.

The reflection of ultrasound from a rough surface interface is dependent on the wavelength of the sound wave relative to the air gaps. When the wavelength of the sound is of a similar size to the air gaps, significant scattering occurs. However, if the wavelength of the signal is long compared to the magnitude of the air gaps, the interface as a whole behaves like a reflector. Tattersall [9] and Kendall & Tabor [10] investigated this case, and found the reflection to be governed by the *spring* like behaviour of the interface. In the study the asperity contacts at the interface were modelled as a series of springs in parallel (Figure 2). The interface then has a stiffness *K* (expressed per unit area), which is defined as the change in nominal contact pressure, p_{nom}, required to cause unit approach of the mean lines of the surfaces. Thus:

$$K = -\frac{dp_{nom}}{du} \tag{1}$$

where *u* is the separation of the mean lines of roughness of the two surfaces. The interfacial stiffness was related to the reflection coefficient, for two similar materials in contact the relation reduces to:

$$|R| = \frac{1}{\sqrt{1+(2K/\omega z)^2}} \tag{2}$$

where ω is the angular frequency (= $2\pi f$) of the ultrasonic wave, and *z* the acoustic impedance (the product of wave speed and density for the material).

Drinkwater et al. [11] assessed the applicability of the *spring* model to ultrasonic reflection data from a series of rough surface contacts. They demonstrated that the model could be applied to ultrasonic reflection data up to frequencies of about 50 MHz,

and that it can also be used to determine information about the nature of the contact at the interface. Its application is however also dependent on the materials and surface roughnesses of the contact under investigation. This may act as a limiting factor before the maximum possible frequency of 50 MHz is reached.

For a given pair of contacting surfaces the interfacial stiffness is dependent on the load applied, and hence the contact pressure between them. When the load is increased, the proximity of the contacting surfaces reduces. This leads to an increased number of asperity contacts at the interface, and the stiffness rises. The interfacial stiffness is a partially linear quantity, and shows some linear behaviour at low load. It varies from zero when the surfaces are just touching, to infinity when the interface is completely conformal. The reflection coefficient then varies from unity to zero.

Unfortunately, interfacial stiffness is not just dependent on the contact pressure between two surfaces. It is also a function of the size, number, and distribution of the asperity contacts at the interface. There is thus no unique single relation between contact pressure and stiffness. However, as demonstrated by Dwyer-Joyce et al. [12], a calibration experiment may be performed to find the relation between interfacial stiffness and contact pressure for a given pair of contacting surfaces. Arakawa [13] and Hodgson et al. [14] showed that at low loads the relationship between stiffness and contact pressure is linear. This provides a method to obtain the contact pressure distribution from a map of the ultrasonic reflection from an interface.

3 Experimental Details

3.1 Transducers and Focusing

In this study a 10 MHz focusing transducer was used to investigate rough surface contacts. An ultrasonic transducer contains an active piezo-electric element, which emits an ultrasonic signal in response to an electrical excitation. The emitted ultrasonic signal contains a range of sound frequencies, and is termed a multi-frequency pulse. Within the pulse emitted, the frequency containing the maximum energy is called the centre frequency. The frequencies surrounding it show a continuously decreasing energy content, as their proximity to the centre frequency increases. The term bandwidth is used to classify the useful frequency range of the transducer. This identifies the frequency range over which information can be determined about the contact by the transducer. Frequencies within the bandwidth are those that have an energy content of at least fifty percent of that at the centre frequency (this value is arbitrarily chosen, it is judged that useful information about the contact cannot be determined from components of the signal with an energy content which is less than fifty percent of that at the centre frequency). Therefore, the bandwidth has an upper and lower boundary. For the 10 MHz transducer used in this study the centre frequency was 8.8 MHz, and the upper and lower limits of the bandwidth 11.5 and 6 MHz respectively. It should be noted that a drop of fifty percent in energy content corresponds to a 6 dB reduction in signal strength.

A large impedance mismatch occurs at a solid-air boundary. Thus, it is extremely difficult to convey an ultrasonic signal to a specimen through an air gap, as the signal will not be transmitted from the transducer into the air. Therefore, a couplant is usually used to convey the ultrasound from the transducer to the specimen under investigation.

Here, de-ionised water was used as a couplant, the de-ionisation process removed any air bubbles that could potentially scatter the sound signal.

In this study, the rough surface contact was investigated using a focused ultrasonic signal. A concave lens is bonded to the front of the transducer; this provides the initial convergence of the sound wave. As shown in Figure 3a, the transducer has a known focal length in water determined by the angle of the lens. When the transducer is moved over a specimen, the sound signal refracts at the boundary as it enters the body, and the focal length changes from that in water (Figure 3b). The refraction of the ultrasound is calculated using:

$$\frac{\sin\theta_i}{\sin\theta_r}=\frac{c_1}{c_2} \tag{3}$$

where θ_i and θ_r are the angles of incidence and refraction, and c_1 and c_2 the speeds of sound in the material before and after the boundary respectively. As the angles of incidence and refraction are known, along with the thickness of the upper specimen, the water path required to focus the ultrasound onto the interface is calculated. The transducer position is then adjusted accordingly (Figure 3c).

The ultrasonic wave is focused to a finite spot size on the interface. The diameter of the focused spot is the resolution of the technique. It is quantified in terms of the bandwidth as follows [15]:

$$SpotDiameter\left(-6\text{dB}\right)=\frac{1.025\,fd_c}{l_w c_w} \tag{4}$$

where c_w and l_w are the speed of sound and the focal length of the transducer in water respectively, and d_c the diameter of the piezo-electric crystal. The focused spot diameter for the 10 MHz transducer used was 0.9mm.

3.2 Experimental Apparatus

As well as the 10 MHz transducer, the ultrasonic equipment consisted of an Ultrasonic Pulser-Receiver (UPR), an oscilloscope, and a desktop PC. A control signal from the UPR triggers the transducer, which then emits the ultrasonic sound wave. The transducer operates in pulse-echo mode; this means the reflected signals are received back by the same transducer. Both the emitted and reflected pulses are displayed on the oscilloscope, from which they can be downloaded to the PC for data processing. A schematic of the equipment set-up is shown in Figure 4, along with an example specimen under inspection. The transducer is positioned in a water bath above it, so as to focus the ultrasonic sound signal onto the interface.

The ultrasonic measurement process is automated using PC controlled stepper motors. These are also marked on Figure 4. The stepper motors control the transducer position, allowing it to be moved over an area. As all the equipment is interfaced using the PC, the transducer can be scanned over a given rough surface contact, recording ultrasonic measurements at discrete intervals. The vertical position of the transducer is set manually.

3.3 Test Specimens

In order to provide a study of the contact pressure in a bolted joint, simple specimens consisting of a plate bolted to a base were manufactured from EN24 steel. Figure 5 shows a simple schematic of the circular test specimens. Two base specimens were manufactured with differing surface finishes. This was done to assess the effect of surface texture on the integrity of the bolted connection. The first base had a ground finish, and the second a turned profile. Both base specimens had an outer diameter of 50

mm and were 15 mm thick. The upper plate had a ground surface finish; it had an outer diameter of 50 mm in diameter and was 10 mm thick. The upper plate was used in all tests. Therefore, the two interfaces under investigation in this study consisted of two ground surfaces loaded together, and a ground surface pressed against a turned profile. The specimens were bolted together using a steel M12 bolt (grade 8.8). Surface profiles, recorded using a stylus profilometer, from the three specimens are shown in Figure 6, these plots demonstrate the different surface topographies of the specimens. The long-range waviness introduced by the turning process is clearly visible on the surface profile taken from the base specimen in Figure 6c; the profile is longer than the others included to illustrate this effect.

3.4 Measurement Procedure

The bolt was tightened and the sample interface scanned using the transducer (as shown in Figure 7a). The transducer and bolted specimens were mounted within the scanning table, with the ultrasonic signal focused on the interface. De-ionised water was used as a couplant between the transducer and the specimens. Ultrasonic scanning was carried out with bolt torques of 30, 40, 50, and 60Nm on each of the two sample interfaces. Scans were also performed with a standard washer inserted under the bolt head, for the rough surface case. The washer was made from hardened steel, and was sized to fit the M12 bolt.

When investigating the sample interfaces the transducer was scanned over the complete contact, and the amplitude of the reflected pulse recorded at 0.25mm intervals. The reflected signal from the interface has a lower value than the emitted pulse; this is because it is partially transmitted at the interface, as well as being attenuated as it travels

to and from the interface in the material bulk. A reference scan is also recorded as shown in Figure 7b. This is done by taking ultrasonic measurements at the same points as before, but with the upper plate absent. The reference trace is only diminished by attenuation, as all the ultrasound is reflected back from the now steel-air interface. If the reflected voltage scan is divided by the reference scan, attenuation is cancelled out. This leaves a map showing the fraction of ultrasound incident at the interface that is reflected from it, in other words a map of reflection coefficient, *R*. In this way reflection coefficient maps were produced for the two different interfaces investigated at a series of different bolt torques. Applying Equation 1 to the reflection coefficient data produced maps of interfacial stiffness for the contact.

The technique presented in this study is the time domain method. In it an assumption is made that the peak amplitudes of both the incident and reflected pulses occur at the centre frequency. Although more time consuming, it is possible to analyse ultrasonic reflection data in the frequency domain [11]. For a given point on the scan the complete reference and reflected pulses are downloaded to the PC, and then converted to the frequency domain using a fast fourier transform (FFT). Reflection coefficient is then determined as a function of frequency by dividing the reflected FFT by the reference FFT. The *spring* model is then applied to the reflection data over the bandwidth of the probe. It is only applied over the bandwidth, as this is the frequency range over which useful information about the contact can be determined. Interfacial stiffness is independent of frequency, and can be determined at this point from the calculated data. This process must be repeated at every point in the scan, and at each loading. The time domain method has been used in this case, as it represents a substantial time saving

when repeatedly scanning large contacts. However, with the advent of faster computer processors in the future, the frequency domain method will become more accessible.

3.5 Calibration

A calibration experiment was performed to find the relationship between interfacial stiffness and contact pressure for the bolted joint specimens. Separate calibrations were performed for the two interfaces under investigation due to their different contact conditions. Figure 8 shows the calibration specimens and the experimental set-up.

The calibration specimens were machined from the same material and treated to the same surface finishing processes, as the interface the calibration was required for. As shown in Figure 9, these specimens were loaded together, with an ultrasonic signal focused at the interface between them. Single point ultrasonic reflection measurements were recorded at a series of known loads. A reference measurement was also recorded with the lower specimen absent. The reflection coefficient along with the interfacial stiffness (using Equation 1) was then calculated at each load. As the contact area between the specimens was known, the contact pressure was determined for each of the loads. This allows a graph to be plotted relating interfacial stiffness to contact pressure. Calibration graphs are shown in Figure 9 for the two bolted joint interfaces. The turned surface is rougher therefore for a given contact pressure the measured stiffness is lower, as the higher the conformity between the surfaces the stiffer the interface.

Over the pressure range shown in Figure 9 the relationship between interfacial stiffness and contact pressure is approximately linear. The linear relationship $p=mK$ was least squares fitted to the data, where p is the contact pressure, K the interfacial stiffness, and m the reciprocal of the gradient of the line (the units of m are MPa/[GPa/micron]). The

constant *m* was determined for the two cases shown in Figure 9, it was found to be 53.5 for the ground interface, and 62.3 for the case of the turned surface pressing against the ground plate.

4 Ultrasonic Results

4.1 Ground Surfaces

Figure 10 shows the contact pressure distribution at the clamped interface for bolt torques of 30, 40, 50, and 60 Nm. As can be seen, the interface is subject to a circular clamping zone around the bolt hole. The majority of the interface load is supported in this area, with a low contact pressure everywhere else. Tightening the bolt increases the load supported at the interface, and leads to an increased intensity in the contact. However, there is no spread of the contact with increased load. As the bolt is tightened the overall size of the contact zone does not grow, and the existing clamped area supports the extra load.

As can be seen the contact pressure distribution is non-symmetrical. This is because one side of the bolt head is clamped down more due to the angular nature of the threads. The effect of this is to give the observed rise in the contact pressure on one side of the clamped zone. The area in the contact zone experiencing the increased clamping force is marked by a series of white arcs on Figure 10. As the bolt is tightened it rotates, this in turn leads to a rotation of the area experiencing the increased clamping force. During the experiment the rotation of the bolt head was measured as the torque was increased from 30 to 60 Nm. The bolt head was found to move through an angle of approximately 90 degrees as it was tightened, this is similar to the overall rotation of the

zone experiencing the increased clamping force that is shown by the white arcs marked on Figure 10.

Figure 11 shows a section of the interface contact pressure distribution at a bolt torque of 30 Nm, the section line is marked A-A in Figure 10. The maximum contact pressure on the interface occurs approximately in line with the edge of the bolt head. It is unsurprising to find that the edge of the bolt influences the pressure profile, as it is a discontinuity that acts as a stress concentration, in turn leading to the increased stress measured on the interface.

4.2 Turned Surfaces

Figure 12a shows the contact pressure distribution at the interface when there is a turned surface profile introduced. The interface consisted of a turned surface clamped up against a ground surface. Figure 12b shows a surface profile from the base specimen, this specimen had a turned finish. The long-range waviness associated with such a surface profile is clearly visible. A similar trace is not shown here from the ground specimen as it was found to be virtually flat at this scale.

As seen in Figure 12a the interface is subject to a circular clamping zone. This is similar to the result seen for the smooth specimens. However, the clamping zone is now dependent on the surface roughness. As shown by Figure 12b the clamping zone is coincident with the surface wave, where the troughs occur in the profile the specimens barely touch. As seen previously the contact zone is still non-symmetrical due to the nature of the thread, and this effect was once more seen to rotate as the bolt was tightened. The peak pressures recorded for a rough interface were higher than those from a smooth one. This was due to the surface roughness giving a less conformal

contact. In this case the roughness increased the total area of contact and reduced the average pressure. This affect is however specific to this roughness profile, and will be different for another case. Away from the clamped zone the average contact pressure was similar to that of the smooth specimens.

4.3 The Effect of a Washer

Figure 13 shows two scans of the turned interface at bolt torques of 50 Nm. Figure 13a show the contact pressure distribution with the bolt clamping the interface together, whereas, Figure 13b shows the interface pressure distribution when a washer is inserted under the bolt head. When comparing the two scans it can be seen that the washer reduces the intensity of the clamped zone, whilst simultaneously increasing the average pressure in the background. The peak pressure in the clamping zone was reduced from 172 MPa to 120 MPa. However, away from the clamped zone without the washer the surfaces were barely touching, with the washer present the average pressure rose to 41 MPa in this area. The washer increases the integrity of the joint giving a more consistent overall clamping of the interface, as it reduces the effect of the roughness.

5 Discussion

It is important to put the results from the ultrasonic investigation into context by comparing them with previous research work in this area. Such work has focused on quantifying the contact pressure distribution using an average line scan, which gives plots showing the pressure variation on a line moving out in a radial direction from the centre of the bolt hole. It was therefore necessary initially to reformat the ultrasonic data

to allow a direct comparison. Details of how this was achieved are given in the next section.

5.1 Average Contact Pressure Distribution

Figure 14 shows line scans taken from the ground interface pressure maps. These were constructed from circumferential averages taken at given distances from the centre of the bolt hole on each scan. They show on average what happens to the contact pressure distribution as the bolt load is increased. Once again it is evident that the position of the peak pressure on the interface is influenced by the edge of the bolt head. A change can also be seen in the contact pressure distribution as the bolt torque is increased past 30 Nm. The contact pressure profile sharpens, with a significantly higher percentage of the joint load supported closer to the bolt hole. This is almost certainly due to the stress concentrating effect of the bolt head starting to dominate as the load increases. At bolt torques in excess of 40 Nm, the form of the interface pressure profile remains constant.

The total load in the bolted joint can be determined from the ultrasonic measurements. It is not calculated for the 30 Nm scan, as Figure 14 shows that all the contact pressure distribution was not captured at this bolt torque. When using the ultrasonic apparatus to scan a bolted interface a limited area can be scanned, unfortunately for the 30 Nm scan it was insufficient to capture the complete pressure distribution. Shigley & Mischke [1] propose the empirical relation between total load and bolt torque:

$$\text{Bolt Torque} = 0.2\, F\, d \tag{5}$$

where F is the total joint load and d the bolt diameter. Table 1 compares the calculated joint loads to those determined ultrasonically for bolt torques of 40, 50, and 60 Nm. As shown the correlation is good.

5.2 Normalised Contact Pressure Distribution

A normalised contact pressure distribution was determined for each of the measured interface pressure profiles by dividing the average contact pressure distributions shown in Figure 14 by the mean stress, q, under the bolt head for that scan (leading to the pressure profile being expressed in terms of the ratio p/q). The mean stress was determined at each bolt torque using the measured pressure map. The map was integrated to find the total joint load, which was then divided by the area under the bolt head to find the mean stress. The distance, r, of the measurement from the centre of the bolt hole was also normalised with respect to the bolt radius, a (leading to the data being spatially characterised in terms of the ratio r/a). Figure 15a shows the normalised line scans at the four different bolt torques investigated for the ground interface. Disregarding the result for 30 Nm, the normalised pressure profiles are coincident. This shows that the interface pressure distribution maintains the same form and grows linearly with increasing load. Therefore, an average normalised profile was determined for the ground interface, as shown in Figure 15b.

Figure 16 compares the normalised pressure distribution for the ground interface, to those from previous studies. The previous work highlighted is for similar materials and relative geometries as this study. Figure 16a compares the average result from this work with that from the ultrasonic study by Ito [8] and data from a numerical model used by Gould & Mikic [5]. While the result from this study has a similar global form to the normalised pressure distribution determined by Ito, there are some clear differences. The overall pressure distribution determined by Ito is higher, and the peak contact pressure occurs at the edge of the bolt hole, where in this study it occurred away from it.

The differences are due to the varying approaches used to take the ultrasonic measurements.

Ito used single point ultrasonic measurements recorded at six prescribed points from the bolt hole and then extrapolated and interpolated to determine the overall profile, which is clearly undesirable. An unfocused ultrasonic transducer was used to investigate the interface, which had a spot diameter of 20mm. This meant measurements close to the bolt hole were impossible, so in this region the data was extrapolated and the peak away from the hole was missed. In the present study a focused ultrasonic signal was employed, with a spot diameter of 0.9mm. Using this transducer gave much greater resolution, and hence better measurements, close to the bolt hole.

The large transducer used also explains the higher pressure profile seen in Ito's work. Due to its size, the transducer still received information from the high pressure area close to the bolt hole, even when centred some distance away from it. This will have led to an artificially increased pressure profile. Further, in Ito's study a non-specific calibration was used to relate the ultrasonic reflections to contact pressure. The work of Drinkwater et al. [11] showed the need for a specific calibration routine when using this type of measurement technique.

Also included in Figure 16a are numerical results determined by Gould & Mikic [5]. The two curves shown from their work were for different bolt head diameters. To allow a valid comparison between the numerical results and the normalised ultrasonic measurement, it is important that the ratio of the diameter of the bolt head to the shank is the same. For the first numerically derived curve presented, the ratio is larger than in this work, and in the second it was smaller. As the ultrasonic test specimens have a ratio for the bolt size in between the two numerical results, it is unsurprising that the

determined curve also falls between them. The numerical results also show peak pressures at the edge of the bolt hole. This effect is probably due to the simplified modelling procedure, where the bolt is removed and modelled as a distributed load. Such a modelling procedure neglects any stress concentration issues associated with the bolt head. Figure 16b shows a numerical result from [6]; in this case the bolt has been included in the finite element model. The normalised pressure distribution has been determined by dividing the load on an individual cell at the interface in the finite element model, by the load applied to the bolt. This produces a distribution of normalised joint load, proportional to the normalised contact pressure. Although the result was normalised in a way that inhibits quantitative comparison with other studies, the peak pressure clearly occurs away from the edge of the bolt hole and is influenced by the edge of the bolt head. This is a similar result to that shown in this study.

5.3 Spread Angle and Joint Member Stiffness

As well as the magnitude of the pressure distribution in a bolted joint, the spread is also important. Typically the spread of the contact is characterised using a pressure cone approach (Figure 17), with the half-apex angle α used to quantify the cone.

Table 2 shows the half-apex angles from the different studies highlighted, along with an analytical solution based on elasticity [1]. As shown, the ultrasonic results for a ground interface compare well with those from previous studies. The work of Ito [2] predicts a greater spread in the contact than seen in this study, which is again attributable to the poor spatial resolution of the transducer used in the work. Table 2 also shows how the turned profile changes the spread of the contact. In this case the roughness profile caused an increase in the spread of the contact. However, it is likely that other

roughness profiles could lead to a larger or smaller spread than observed in the ground case.

In this study the half-apex angle has been determined for a specific case. Shigley & Mischke [1] predicts the spread of the contact to be independent of geometry, roughness or material, and determined only by the bolt size and half-apex angle. However, this is a very simplistic approach and has not been validated experimentally, and further work is required to assess the affect of these factors on the half-apex angle. Indeed this study clearly shows there is an influence due to surface finish on the contact spread. As all the numerical and analytical studies assume perfectly smooth surfaces, this appears to be a limiting factor in this type of investigation.

Shigley [1] also proposes an analytical solution for calculating the joint member stiffness:

$$\frac{k_m}{Ed} = \frac{\pi \tan\alpha}{2\ln\left[\frac{\left(l\tan\alpha + d_w - d\right)\left(d_w + d\right)}{\left(l\tan\alpha + d_w + d\right)\left(d_w - d\right)}\right]} \tag{6}$$

where k_m is the joint member stiffness, E the Young's modulus of the clamped material, d the bolt diameter, d_w the diameter of the contact under the bolt head, and l the effective grip. Equation 6 is presented in a dimensionless form, with the geometry factors highlighted shown schematically in Figure 18.

Equation 6 was applied to the bolted joint geometry investigated in this study, and a graph was plotted relating the dimensionless joint member stiffness to the half-apex angle (Figure 19).

As shown in Figure 19, the dimensionless stiffness is highly dependent on the half-apex angle. Also marked on the Figure are three values for the half-apex angle, these are the values of 41 and 68 degrees from this study, along with the 30 degrees recommended by

Shigley [1]. Clearly the dimensionless stiffness is highly sensitive to the value of half-apex angle selected; where the difference is minimal between angles of 30 and 41 degrees, between 30 and 68 degrees the joint stiffness more than doubles. In reality bolted surfaces are likely to be rough, if this is ignored and at the design stage an incorrect assumption is made as to the spread of the contact, a large error will be present in the joint stiffness calculation. This study clearly shows the influence of roughness on the spread of the contact, and the need for the inclusion of a correct half-apex angle when calculating the joint stiffness for use in fatigue calculations.

5.4 Transducer Focusing and Scanning

The ultrasonic method is best applied to a large contact with gradual pressure variations, like the bolted joint in this study. This is because the technique is limited by the size of the focused ultrasonic spot. There may be significant problems in applying the method to a small contact with rapidly changing pressure contours, as it would be difficult to resolve the pressure distribution. It is possible to use higher frequency ultrasound in such cases, as the focused spot reduces in diameter with increasing frequency. However, the attenuation also increases at higher frequencies, leading to a vastly reduced reflected signal.

6 CONCLUSIONS

- A method has been established to determine interface pressure in a bolted joint. The method uses reflected ultrasonic measurements and a parallel calibration procedure. The interface pressure distribution has been determined for ground interface

- The experimental results show an increase in joint load as the bolt is tightened. There is, however, no spread of the contact as the bolt torque is increased. It was found that the introduction of a turned profile fragmented the contact, resulting in a larger contact spread with higher peak pressures than the ground surface case. A washer was found to increase the bolt clamping performance when used for the turned surface case.
- Good agreement was found when comparing the ultrasonic measurements to previous studies, with respect to the spread of the contact pressure distribution. However, in this study the peak contact pressure was found to occur away from the edge of the bolt hole, and to be influenced by the edge of the bolt head. This contrasts with previous work, and is likely to be due to simplifying assumptions made in those studies.
- The surface roughness profile can lead to significant changes in the spread of the contact, which is a critical parameter in determining joint stiffness used in fatigue calculations. Some studies recommend a single estimate of the contact spread regardless of the surface finish. This study highlights the need to correctly estimate the spread of the contact, as it can significantly affect the joint member stiffness.
- The method is limited by the resolution of the ultrasonic technique. Currently contact pressures are averaged over a 1mm diameter, which is the focused spot size of the transducer.

7 REFERENCES

[1] Shigley, J.E. and Mischke, C.R. (2001) *Mechanical Engineering Design*, Sixth Edition McGraw-Hill, Singapore.

[2] Lee, S., Song., S., Moran., K. P., Yoovanovich., M. M. (1993) Analytical modelling of thermal resistance in bolted joints. *Proc. of ASME Conference on Enhanced Cooling Techniques for Electronics Applications*, ASME, HTD-Vol. 263, 115-122.

[3] Fernlund, I. (1970) Druckverteilung zwischen dichtflächen an verscrabten flanschen. *Konstuktion* **22**, 218-224.

[4] Greenwood, J.A. (1964) The elastic stresses produced in the mid-plane of a slab by pressure applied symmetrically at its surfaces. *Proceedings of the Cambridge Philosophical Society, Cambridge, England* **60**, 159-169.

[5] Gould, H.H. and Mikic, B.B. (1972) Areas of contact pressure distribution in bolted joints. *Trans. ASME, Series B, J. Eng for Industry* **94**, 864-870.

[6] Ziada, H.H. and Abd El Latyif, A.K. (1980) Loads, pressure distribution and contact area in bolted joints. *Proceedings of the Institution of Engineers (India), Journal of Mechanical Engineering* **61**, 93-100.

[7] Sawa, T., Kumano, H., Morohoshi, T. (1996) The contact stress in bolted joint with a threaded bolt. *Experimental Mechanics* **36**, 17-23

[8] Ito, Y., Toyoda, J.M. Nagata, S. (1977) Interface pressure distribution in a bolt-flange assembly. ASME Paper No. 77-WA/DE-11.

[9] Tattersall, A.G. (1973) the ultrasonic pulse-echo technique as applied to adhesion testing. *J. Phys. D: Appl. Phys* **6**, 819-832.

[10] Kendall, K. and Tabor, D. (1971) An ultrasonic study of the area of contact between stationary and sliding surfaces. *Proceedings of the Royal Society, Series A* **323**, 321-340.

[11] Drinkwater, B.W., Dwyer-Joyce, R.S., Cawley, P. (1996) A study of the interaction between ultrasound and a partially contacting solid-solid interface, *Proceedings of the Royal Society Series A* **452**, 2613-2628.

[12] Dwyer-Joyce, R.S. and Drinkwater, B.W. (1998) Analysis of contact pressure using ultrasonic reflection. *Experimental Mechanics, Proceedings of 11th Annual Conference on Experimental Mechanics*, Balkema, Rotterdam, 747-754.

[13] Arakawa, T. (1983) A study of the transmission of elastic waves by a periodic array of cracks. M*ater. Eval*. **41**, 714-719.

[14] Hodgson, K., Dwyer-Joyce, R.S., Drinkwater, B.W. (2000) Ultrasound as an experimental tool for investigating engineering contacts. *Proceedings of the 9th Nordic Symposium on Tribology, 'Nordic 2000'*, Eds. Andersson, P., Ronkainen, H., Holmberg, K., **2**, 377-386.

[15] Krautkrämer, J. and Krautkrämer, H. (1990) *Ultrasonic Testing of Materials*, Springer Verlag.

Figure Captions

Figure 1 Schematic Diagram of a (a) Rough Surface; (b) Rough Surface Contact

Figure 2 Schematic Representation of an Interface using the *Spring* Model

Figure 3 Transducer Focusing (a) Focal Length in Water; (b) Refraction at a Boundary; (c) Focusing at the Interface

Figure 4 Ultrasonic Apparatus

Figure 5 Schematic of Bolted Joint Specimens

Figure 6 Interface Surface Profiles (a) Upper Plate; (b) Ground Base; (c) Turned Base

Figure 7 Ultrasonic Scanning. (a) Loaded Case; (b) Reference Scan

Figure 8 Calibration Specimens and Experimental Set-up

Figure 9 Interfacial Stiffness-Contact Pressure Calibration (a) Ground-Ground Interface; (b) Turned-Ground Interface

Figure 10 Contact Pressure Maps of a Bolted Joint at a Series of Bolt Torques (the circles represent the hole diameter)

Figure 11 Contact Pressure for Section Line A-A at 30 Nm

Figure 12 (a) Pressure Map at a Torque of 60 Nm for a Turned Interface; (b) Surface Profile taken on Section Line A-A

Figure 13 (a) Bolted Turned Interface at 50 Nm. (b) Bolted Turned Interface with a Washer at 50 Nm

Figure 14 Average Contact Pressure Line Scans

Figure 15 (a) Normalised Pressure Distributions; (b) Mean Normalised Pressure Distribution

Figure 16 Published Studies of Bolted Joint Pressure Distributions (a) Normalised Pressure Distribution; (b) Normalised Joint Load Distribution

Figure 17 Pressure Cone Approach

Figure 18 Joint Member Stiffness Calculation Geometry.

Figure 19 Dimensionless Stiffness vs. Half-Apex Angle.

Table Captions

Table 1 Comparison of Measured and Theoretical Total Joint Load

Table 2 Pressure Cone Angles

Figure 1

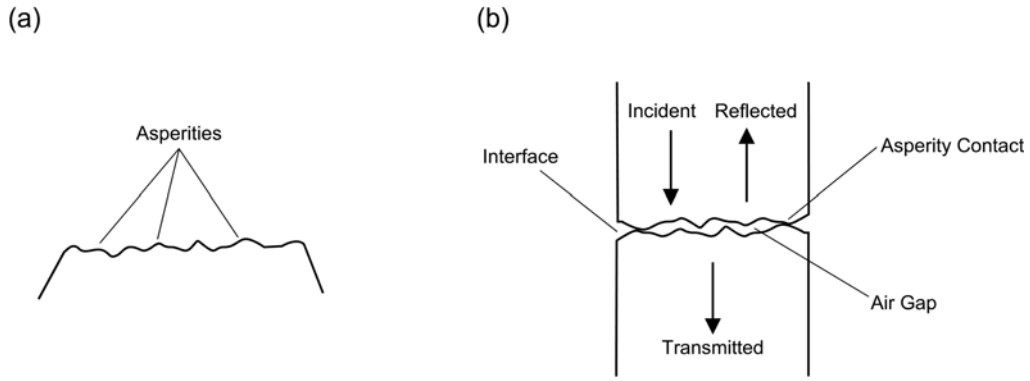

Figure 2

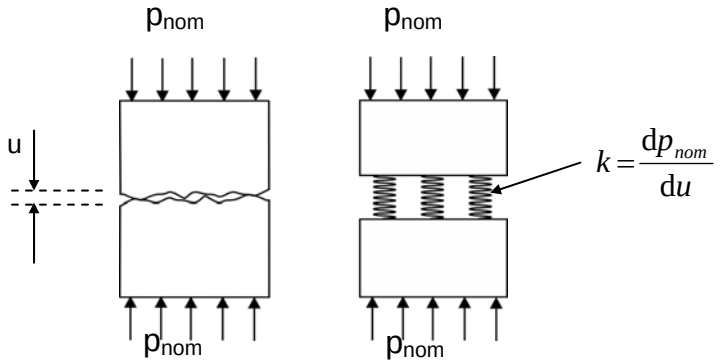

Figure 3

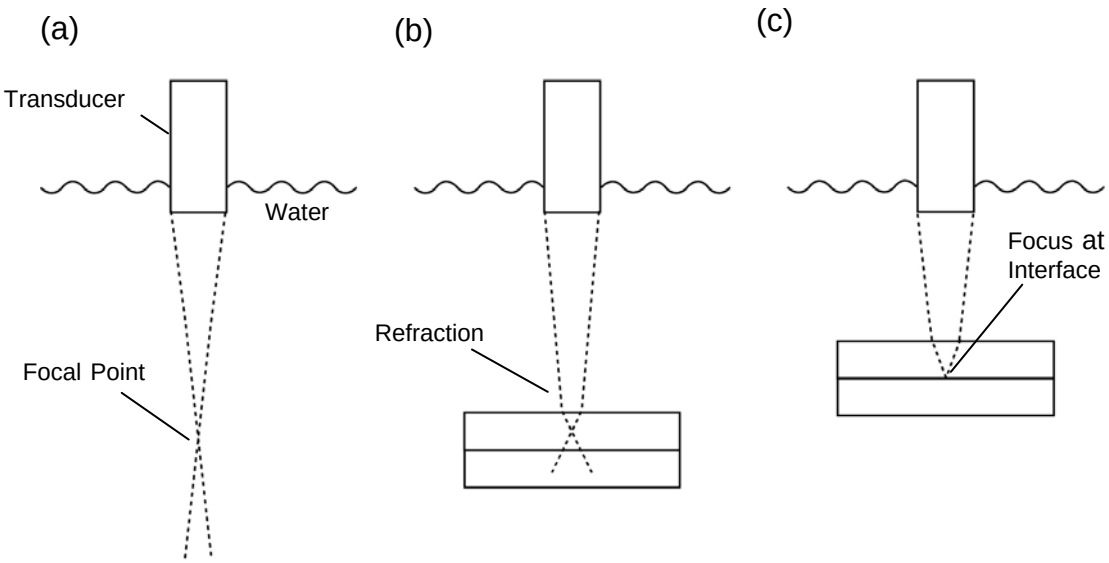

Figure 4

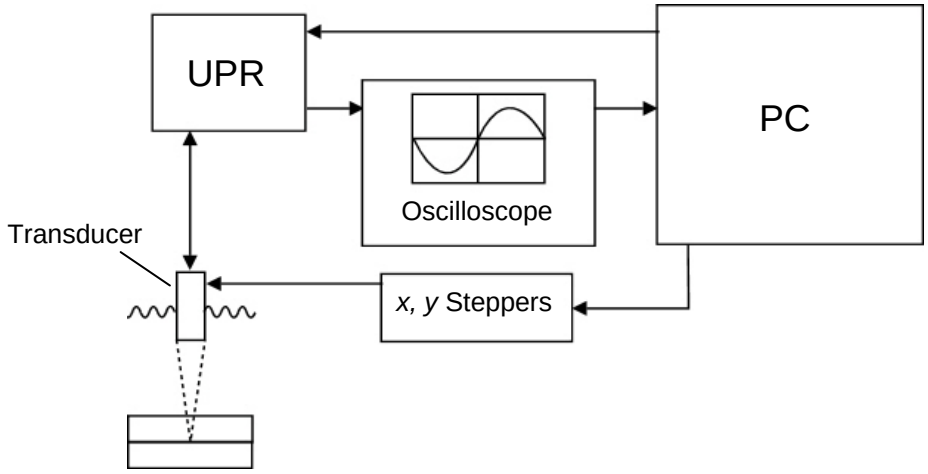

Figure 5

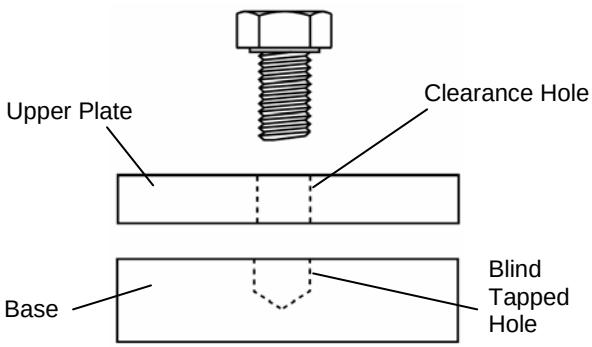

Figure 6

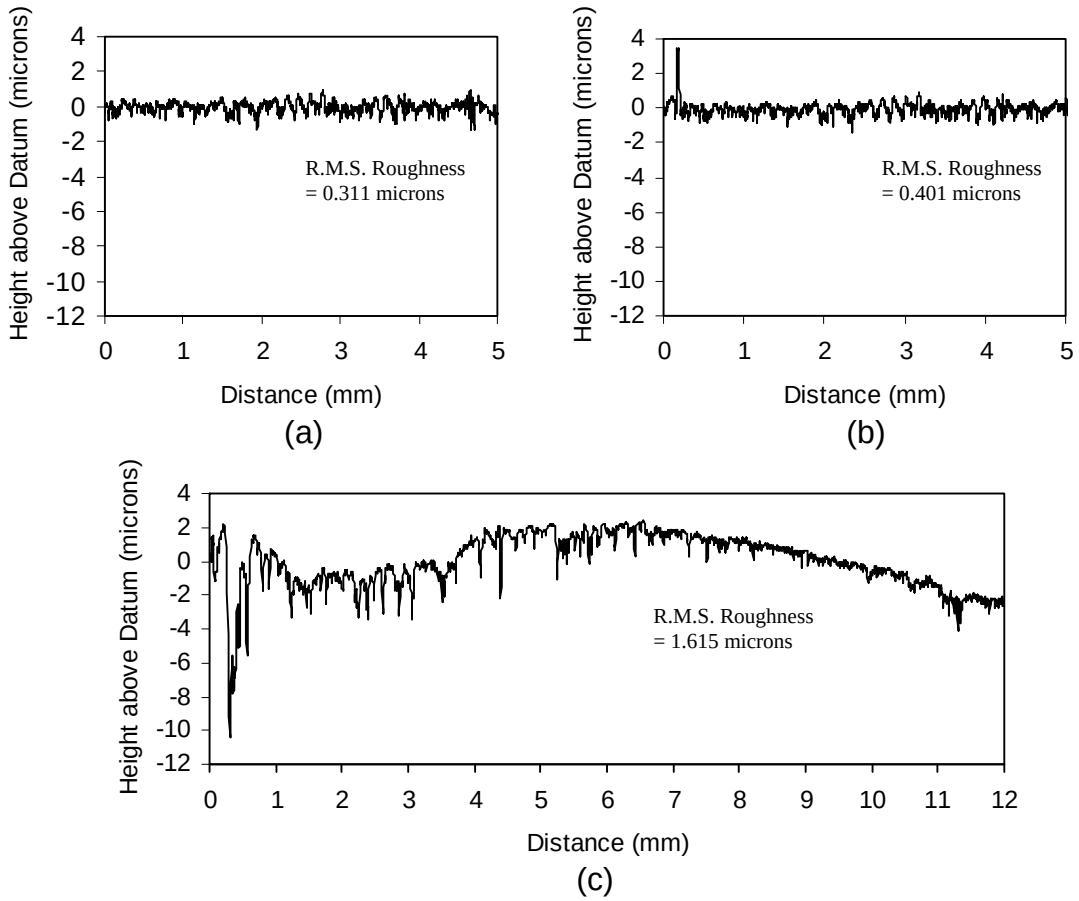

Figure 7

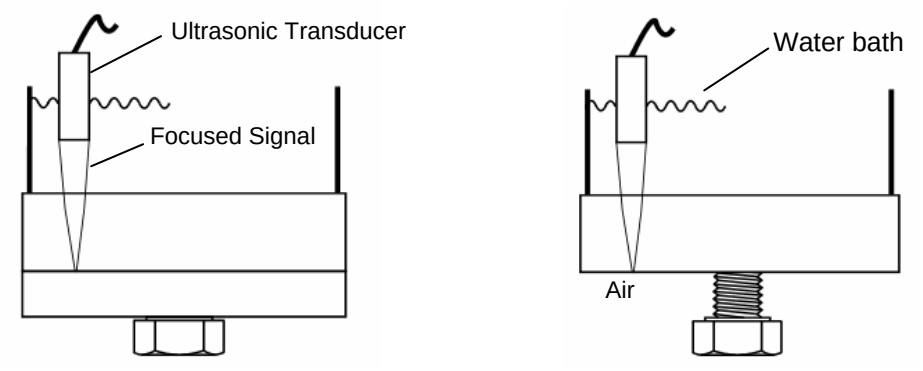

Figure 8

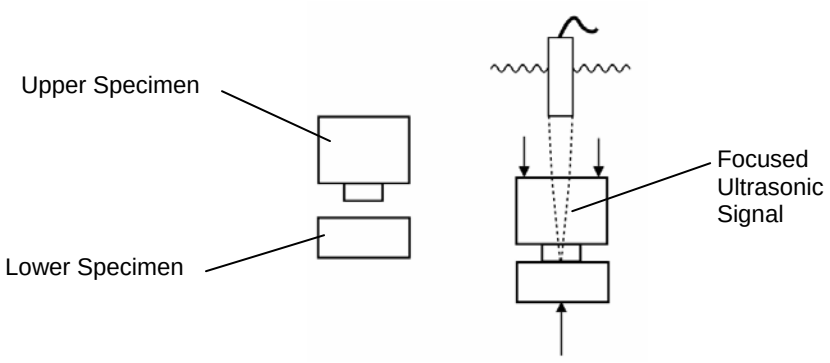

Figure 9

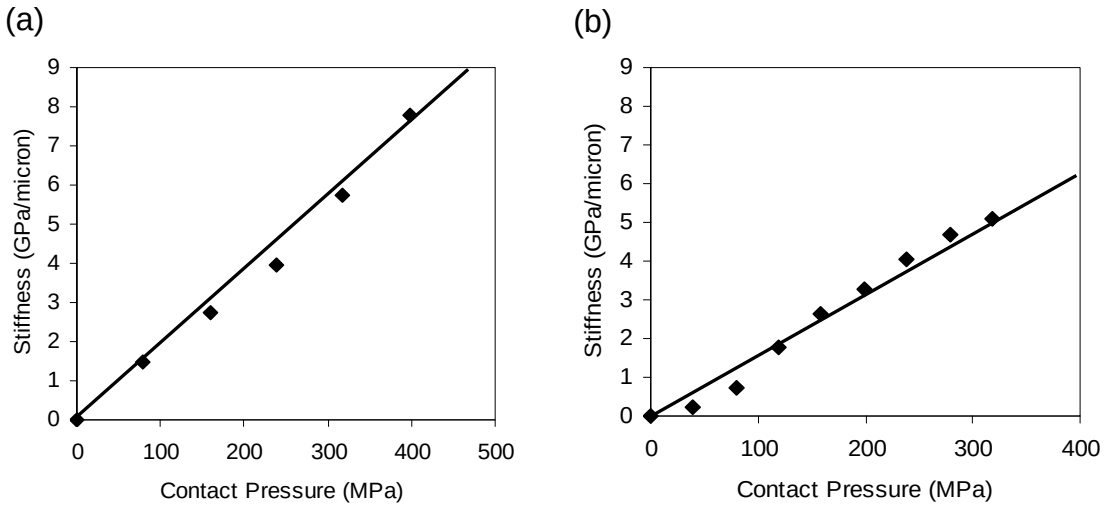

Figure 10

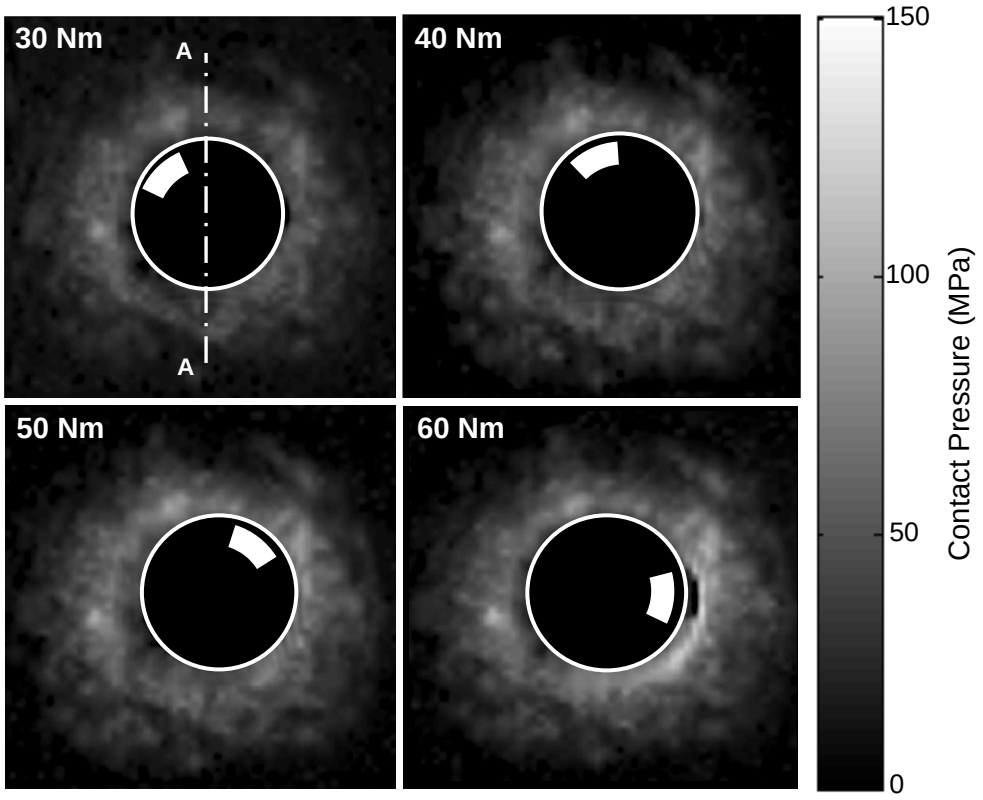

Figure 11

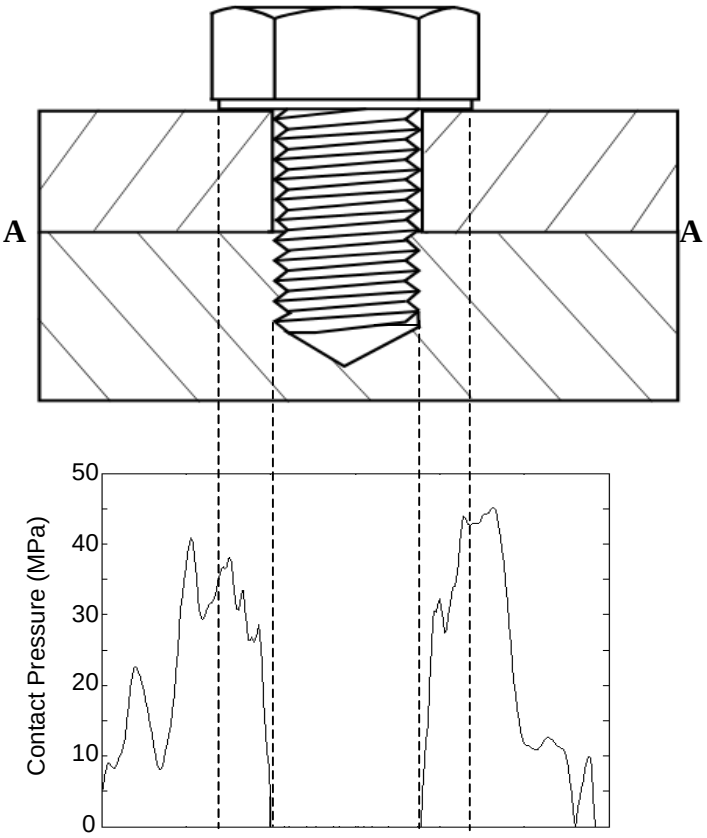

Figure 12

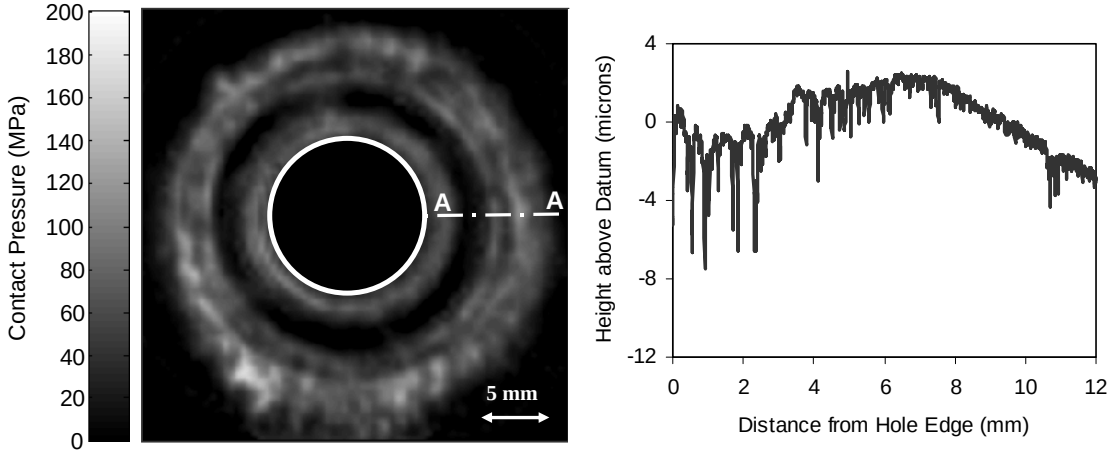

(a) (b)

Figure 13

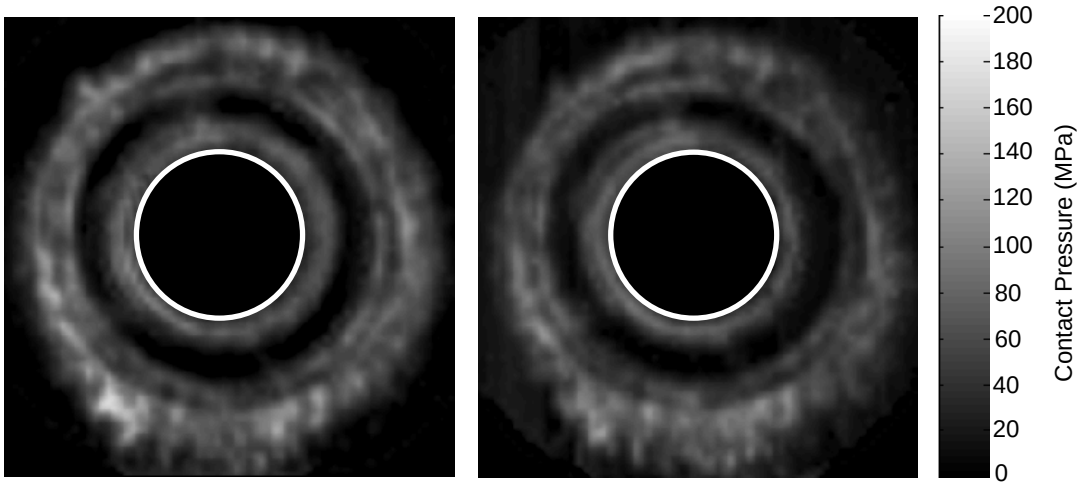

Figure 14

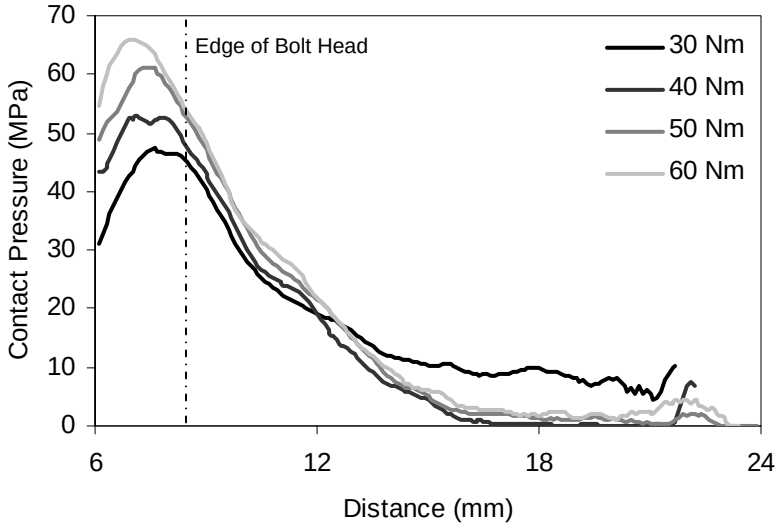

Figure 15

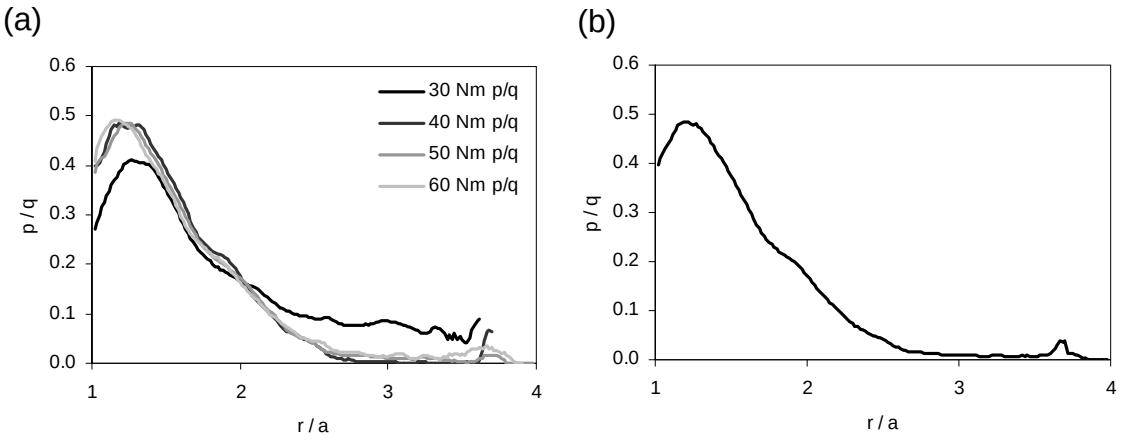

Figure 16

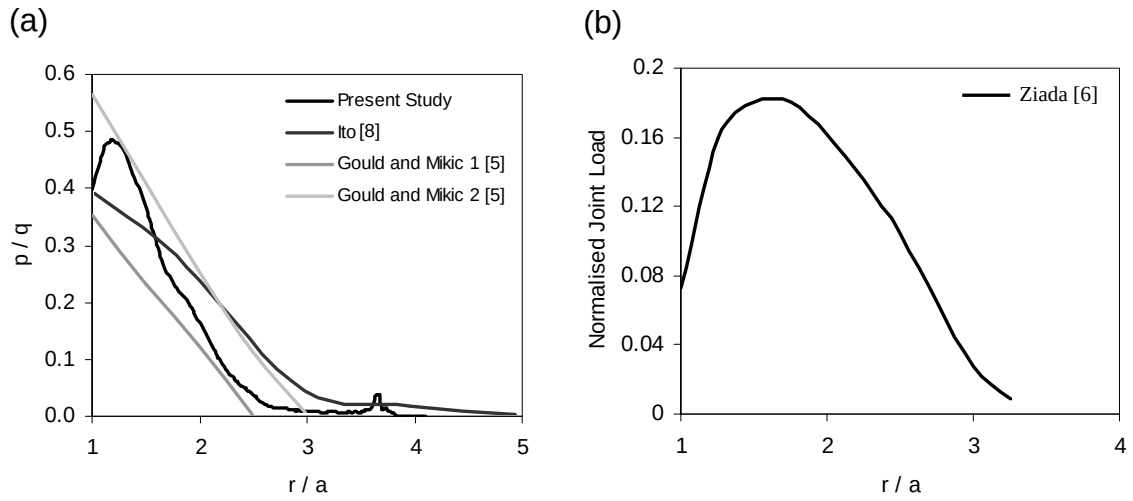

Figure 17

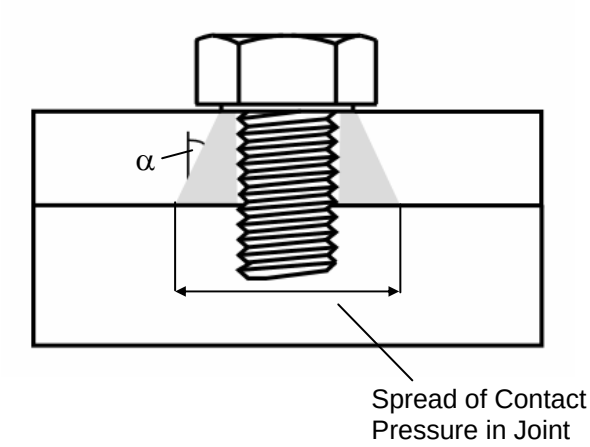

Figure 18

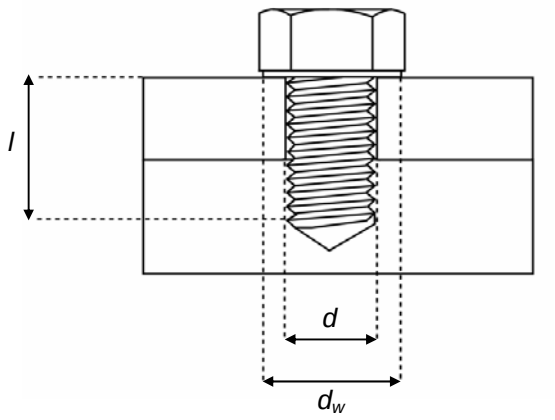

Figure 19

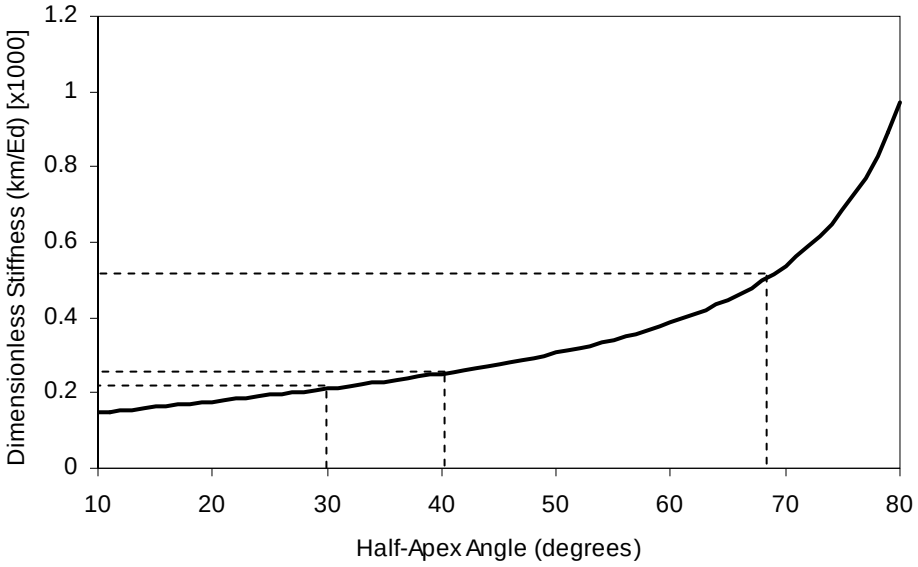
Dimensionless Stiffness (km/Ed) [x1000]
1.2
1
0.8
0.6
0.4
0.2
0
10
20
30
40
50
60
70
80
Half-Apex Angle (degrees)

Table 1

Bolt Torque (Nm)	Measured Load (kN)	Theoretical Load (kN)
30	17.3	16.7
40	20.0	20.8
50	21.2	25.0

Table 2

Originator	Surface Type	Technique	Half Apex Angle
Present Study	Ground	Ultrasonic Scanning	$\alpha = 41°$
Present Study	Turned - Ground	Ultrasonic Scanning	$\alpha = 68°$
Shigley [1]	Any	Elastic Analysis	$\alpha = 30°$
Ito [2]	Ground	Single Point Ultrasonic Measurement	$\alpha \sim 70°$
Gould & Mikic [5]	Smooth	Numerical Analysis	$\alpha = 38°$